metals

MDPI

Article

Bubble Phenomena and Bubble Properties for Horizontal and Vertical Carbon Anode Surfaces in Cryolite Melt Applying a See-Through Cell

Nikolina Stanic [1], Ana Maria Martinez [2], Kristian Etienne Einarsrud [1] and Espen Sandnes [1,*]

[1] Department of Materials Science and Engineering, Norwegian University of Science and Technology NTNU, NO-7491 Trondheim, Norway; nikolina.stanic@ntnu.no (N.S.); kristian.e.einarsrud@ntnu.no (K.E.E.)
[2] SINTEF Industry, 7034 Trondheim, Norway; AnaMaria.martinez@sintef.no
* Correspondence: espen.sandnes@ntnu.no; Tel.: +47-48606478

Abstract: Gas bubble behavior on a carbon anode in a cryolite melt has been studied using a see-through cell. The phenomena studied have been growth, coalescence, detachment, and wetting during electrolysis. The surface orientation affects bubble behavior. Therefore, two different anode designs were tested, an anode with a horizontal downward-facing surface and an anode with a vertical surface. At the horizontal anode, it was found that one large bubble was formed by the growth and coalescence of smaller bubbles, and finally, the large bubble detached periodically. For the vertical anode surface, the detaching bubbles were smaller, and most of them had been going through a coalescence process prior to detachment. The bubbles detached randomly. The coalescence process from the initiation to the final bubble shape at the vertical surface took about 0.016–0.024 s. The current density did not affect the duration of the coalescence. The bubble diameter was decreasing with increasing current density for both anodes. The values were in the range 7.2 to 5.7 mm for the horizontal anode in the current density interval 0.2–1.0 A cm^{-2} and in the range 3.7 mm to 1.5 mm for the vertical anode in the current density interval 0.1–2.0 A cm^{-2}. The wetting contact angle for the vertical anode stayed more or less constant with an increase in current density, which likely can be attributed to the decreasing bubble size rather than an increase in polarization. In addition to the bubble phenomena described and bubble properties found, the impact of the results for better design of laboratory-scale studies is discussed.

Keywords: carbon anode; cryolite melt; bubble behavior; see-through cell; wetting

Citation: Stanic, N.; Martinez, A.M.; Einarsrud, K.E.; Sandnes, E. Bubble Phenomena and Bubble Properties for Horizontal and Vertical Carbon Anode Surfaces in Cryolite Melt Applying a See-Through Cell. *Metals* **2021**, *11*, 965. https://doi.org/10.3390/met11060965

Academic Editors: Eric D. van Hullebusch, João Pedro Oliveira, Belén Díaz Fernández, Leszek Adam Dobrzański, Jae-chun Lee and Alex Lanzutti

Received: 4 May 2021
Accepted: 11 June 2021
Published: 16 June 2021

1. Introduction

Industrial production of aluminum is performed by the Hall–Héroult process in which alumina is dissolved in a molten bath consisting mainly of cryolite, which is predominantly used because of its capacity as a solvent for alumina and fairly suitable ionic conductivity. Aluminum-containing bath species are reduced at the aluminum cathode, forming molten aluminum, while CO_2 is formed in the anode reaction with oxygen-containing bath species and the anode carbon as reactants [1–3]. Gas present at the anode surface contributes to an increased cell voltage. The extra voltage drop in an industrial cell due to the presence of bubbles is about 0.15–0.35 V out of a typical total cell voltage of ~4.5 V [4]. The presence of gas bubbles under the anode contributes to the overall bath resistance because the gas is non-conducting. Accordingly, models have been developed for calculating the resistance effect based on the average layer thickness and fractional surface coverage of the surface. An expression for the additional voltage drop caused by gas bubbles that are applied in numerous cell models has been developed by Hyde and Welch [5]. It expresses the voltage

drop in terms of the anodic current density, electrolyte conductivity, average bubble layer thickness, and anode fraction covered by bubbles and is given by:

$$V_{bubble} = \frac{i_a}{\kappa} \cdot \left[\frac{d_b}{(1-\phi)} - d_b \right] \quad (1)$$

where i_a is the anodic current density in A cm^{-2}, κ is the conductivity in Ω^{-1} cm^{-1}, d_b is the bubble thickness in cm, and Φ is the fraction of anode covered by bubbles.

Haupin [6] verified that the analysis and Equation (1) by Hyde and Welch could also be used for calculating the average bubble layer thickness under the anodes by:

$$d_b = \left[\frac{(0.5517 + i_a)}{(1 + 2.167 \cdot i_a)} \right] \quad (2)$$

The average data reported for gas coverage under the anodes that are predominantly horizontally orientated are in the range of 40–80%, the thickness of the gas bubble layer is 0.5–0.7 cm, and the bubble size is 100–120 cm [3]. The rate of release of the bubbles is also dependent on the path they have to travel and also the angle of the surface from the horizontal. To obtain faster gas bubble release, slotted anode designs have been introduced. With the use of slotted anodes, these parameters have therefore changed, and the bubble layer resistance has been reduced.

Anode bubble behavior for different anode designs and materials has been studied industrially and also on a laboratory scale. The present work examines more closely the bubble behavior for lab-scale anodes typically used to study reaction kinetics and mass transport, anode effect phenomena, current efficiency, kinetics for different carbon quality, wetting, etc. To study bubble behavior in more detail is of importance because bubble behavior affects all the above-mentioned features. Bubbles studies are very important in order to improve proposed models for electrolytic aluminum metal production, e.g., the work by Einarsrud et al. [7], which ultimately can be used to improve the industrial process. Lab-scale experiments are crucial for better understanding key phenomena.

Several researchers [8–12] studied the bubble life cycle, which includes processes as bubble nucleation, bubble growth, bubble coalescence, and bubble detachment on a downward-facing horizontal carbon anode surface applying a transparent cell capturing images from the side openings combined with the observation from above [8,9], side openings only [10], and side and bottom openings [11]. Cassayre et al. [8,9] reported that small individual spherical bubbles were formed at the horizontal anode surface (Ø 9 mm). The bubbles grew and coalesced to form larger bubbles, eventually covering the majority of the anode surface. After reaching maximum size, the bubble was sliding toward the edge of the anode, where it was detached and rose vertically. After bubble detachment, the bubble-free part of the anode surface was available for a new bubble cycle of bubble nucleation, grow, coalescence and detachment. Bubble behavior has also been observed on a vertical anode surface only in a few studies. Cassayre et al. [8,9] studied bubble formation on the verticals side of a graphite anode cylinder at lower current densities (0.05–0.2 A cm^{-2}). It was found that bubble nucleation occurs on specific nucleation sites. The number of nucleation sites grew with the increase in current density. Spherical-shaped bubbles grew and coalesced until reaching 23 mm in diameter, then detached and escaped vertically. The surface coverage was found to be very high, and the small bubbles appeared stuck to the anode.

Kiss et al. [13] studied the detachment of air bubbles from downward-facing horizontal and inclined plates in transparent water tanks. Bubbles are generated at the nucleation sites. They continue to grow there, and after they reach a certain size, they detach from the surface. During bubble growth, an equilibrium exists between the forces that retain the bubble at the nucleation site and the forces that try to remove the bubble. This equilibrium evolves with the increasing volume of the bubble to the point when the detachment forces overcome the retaining forces. For the detachment process, besides the volume of the

bubble, the equilibrium depends on geometry and orientation of the surface, flow-induced forces, etc. Bubble detachment from the surface and departure from the nucleation site does not coincide for every surface orientation. For the horizontal surface facing upward, the bubble detachment from the nucleation site and its departure from the surface typically coincides but for the horizontal surface facing downward or for the vertical surface, the bubble detachment and departure do not have to coincide. On these vertical and horizontal downward-facing surfaces, bubbles can move away from the nuclear site (depart by slow, creeping motion), but to finally leave the surface (detachment from the surface) can occur later. The main detachment force is due to the buoyancy effect. The movement of the liquid exerts another important detachment force, a drag force.

In a liquid, bubbles try to maintain a spherical shape. The driving force behind this shape is the surface tension contracting the bubble to the smallest possible area. When a bubble is moving through a liquid, it can lose its spherical shape because the forces pushing on the bubble from the outside change as it moves through a liquid. Bubble deformation occurs under the effect of gravity and drag forces. Haberman and Morton [14] observed three types of bubble shapes: spherical, ellipsoidal, and spherical cap for vertically rising bubbles in different liquids.

Zawala et al. [15] studied bubble bouncing at a clean water surface. When a bubble is rising upwards in a liquid and approaches a flat free surface with a large enough velocity, a film of liquid is trapped, creating a pressure build-up in the bubble. The liquid film in time breaks, and the bubble bursts through the free surface, causing small droplets of the liquid phase to be propelled into the air, and smaller bubbles can also form in the liquid phase. This bubble bursting phenomenon occurs faster, whereas bouncing usually takes more time [16].

Interfacial tension is the force of attraction between the molecules at an interface. At the gas/liquid interface, this force is often referred to as surface tension. Surface tensions determine the geometry of the bubble. A contact angle (also referred to as a wetting angle) is defined geometrically as the angle formed by a liquid at the three-phase boundary where a liquid (l), gas (g), and solid (s) intersect (Figure 1). The interfacial tensions form the equilibrium contact angle of wetting (θ), which is described by the Young equation:

$$\cos\theta = \frac{\left(\gamma_{lg} - \gamma_{lg}\right)}{\gamma_{lg}} \tag{3}$$

where θ is the contact angle and γ is interfacial tension with the l, s, and g subscript corresponding to liquid, solid, and gas, respectively.

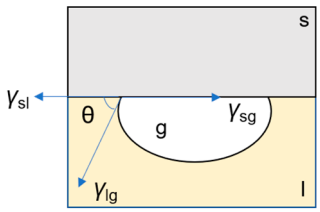

Figure 1. Contact angle (θ) and surface tensions (γ) of gas bubble (g) in liquid (l) underneath the solid (s).

Contact angle hysteresis (wetting hysteresis) is a change in contact angle due to movement of the triple line (a line on the surface where solid, liquid, and gas can all coexist in equilibrium) along the solid surface (Figure 2). The advancing contact angle, θ_a (wetting angle), can be defined as the contact angle at the location where the gas phase is displaced by the liquid. The receding angle, θ_r (de-wetting angle), is then defined as the contact angle at the location where the liquid is displaced by the gas. Contact angle hysteresis is the difference between advancing and receding contact angles.

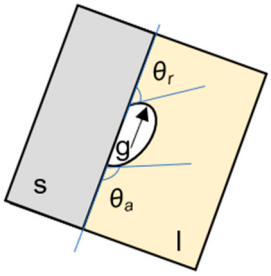

Figure 2. Advancing (θ_a) and receding (θ_r) contact angles for a gas bubble at the three-phase boundary where a liquid (l), gas (g), and solid (s) intersect.

The aim of the current work was to study bubble formation and detachment for two typical anode designs used in lab studies, a horizontal (facing downward) electrode surface and a vertical electrode surface. Video recordings during electrolysis were performed in a see-through cell. The results obtained in this work can not be directly applied to an industrial setting, but the increased knowledge of the bubble behavior is useful for further studies, especially in laboratory-scale studies applying similar anode designs.

2. Experimental Part—Materials and Methods

2.1. See-Through Cell

The experiments were conducted in the see-through furnace shown in Figure 3a. In Figure 3b is shown a principle sketch of the experimental setup. Video recording was performed from the side. The furnace has two side openings that are closed with lids. The lids are removed and replaced with quartz windows only during video recording in order to reduce heat loss. The quartz crucible was resting at an alumina tower construction that was used to adjust the height level of the crucible. The alumina tower was placed in a ceramic crucible whose function was to catch the bath in case of crucible breakage during the experiment.

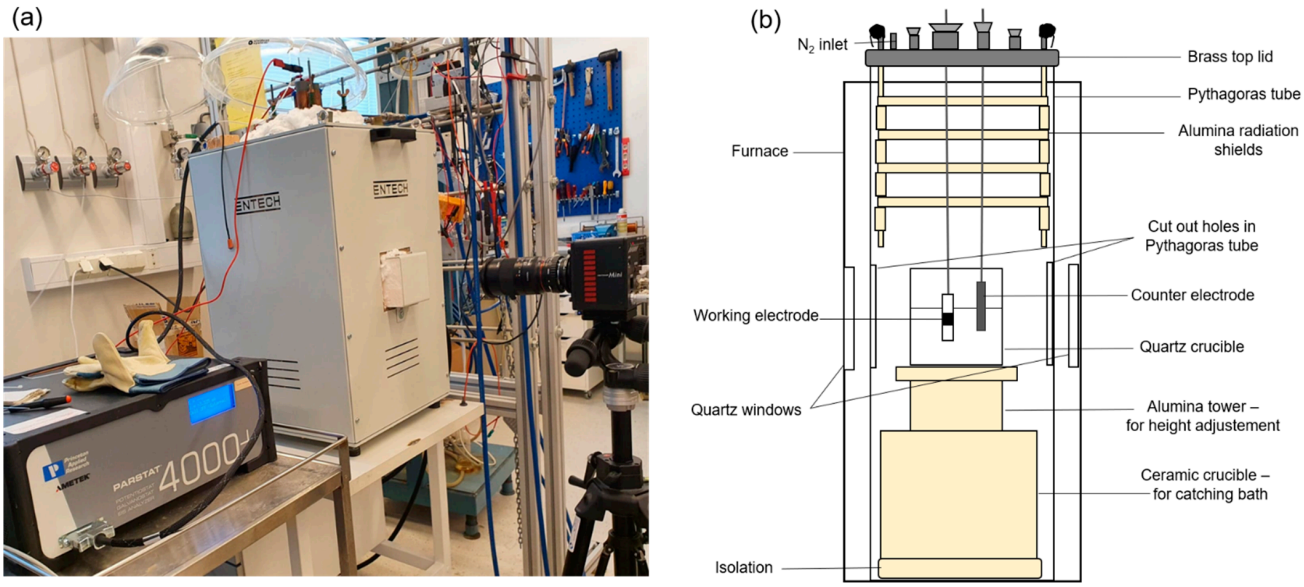

Figure 3. (**a**) The see-through furnace, the potentiostat, and the high-speed camera, (**b**) principle sketch of the interior of the furnace.

2.2. Bath Composition and Temperature

Experiments were performed in a cryolite bath at a temperature of 890 ± 10 °C. The bath composition used in this study is listed in Table 1. The calculated liquidus temperature was 838 °C. The following empirical equation was used for the calculation of the liquidus temperature [1]:

$$\begin{gathered} t = 1011 + 0.14(mas\%AlF_3) - 0.071(mass\%AlF_2)^{2.5} + 0.0051(mass\%AlF_3)^3 - \\ 10(mass\%LiF_3) + 0.736(mass\%LiF)^{1.3} + 0.063((mass\%AlF_3) \times (mass\%LiF))^{1.1} - \\ 3.19(mass\%CaF_2) + 0.03(mass\%CaF_2)^2 + 0.27((mass\%AlF_3) \times (mass\%CaF_2))^{0.7} \\ - 12.2(mass\%Al_2O_3) + 4.75(mass\%Al_2O_3)^{1.2} \end{gathered} \quad (4)$$

Table 1. Cryolite bath composition.

-	wt%	Specification	Producer
Al_2O_3	3	γ-alumina	Merck
AlF_3	15	sublimed "in house"	Industrial grade
LiF	15	purum	Riedel-de-Haën
CaF_2	5	precipitated pure	Merck
Cryolite	62	synthetic, purity >97%	Sigma-Aldrich

Equation (4) agrees reasonably with the literature data [17].

It was crucial to introduce additives to the cryolite-based bath in order to reduce the liquidus temperature and to increase the service time of the quartz crucible. LiF was added to obtain this low temperature, and in addition, it was observed that LiF helped to reduce the fumes inside the furnace and, with that, improved total visibility. The superheat was on purpose kept this large in order to avoid bath freeze due to frequent openings of the furnace side lids and to prolong the video recording time. The bath was contained in the quartz crucible with a wall thickness of 2 mm. The crucible lifetime was a maximum of 5–6 h, including the heating process, which took a minimum of 2 h. The quartz crucible normally broke down due to a formation of holes in the quartz wall at the bath meniscus. On heating, when a temperature of 890 °C was achieved, the side lids of the furnace were removed and replaced with the quartz windows. After some time (approximately 20–30 min), the bath started to freeze on the quartz walls due to heat loss. This was associated with a reduction in bath temperature. The quartz windows were removed and replaced with the side lids. If necessary, the set point of the furnace power supply was increased by 5–10 °C. After 15 min the side lids were removed, and the quartz crucible and bath were checked for transparency in order to continue the experiment.

2.3. Anode Material and Design

Two anode designs, one horizontal and one with a vertical surface and with the same dimensional length (10 mm), were applied. The horizontal anode and the vertical anode are shown in Figure 4. Both anodes were created as described in [18]. A purified graphite material (Schunk Tokai Scandinavia, AB, Trollhättan, Sweden) was the active electrode material. Boron nitride (BN) (BN5000, Kennametal, Newport, UK) was used for anode shielding. The immersion depth of the carbon surface of the anodes was around 3.5 cm. As a counter electrode, a stainless steel (SS) rod with a diameter of 5 mm was used. The SS rod was immersed around 4 cm into the bath, which provided an area of approximately 6.5 cm^2.

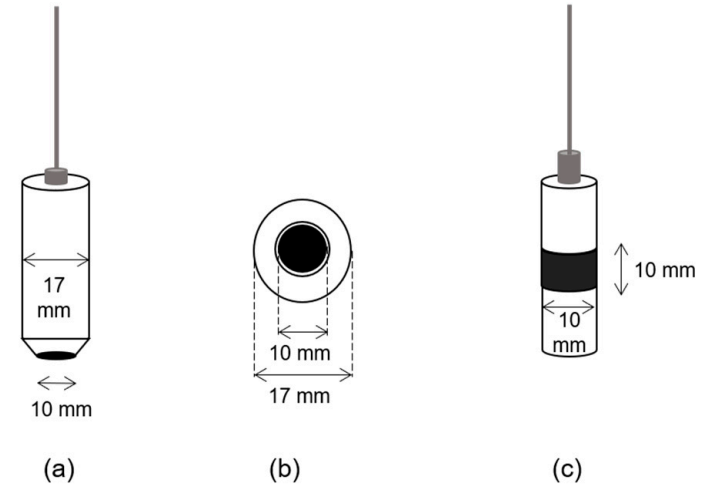

Figure 4. Anode designs with the same dimensional length of 10 mm; (**a**) the horizontal anode with surface area 0.79 cm^2 45 degrees angle chamfered boron nitride edges (with small BN shielding around carbon surface, less than 1 mm), (**b**) the horizontal anode shown from below and (**c**) the vertical anode with surface area 3.14 cm^2.

2.4. Experimental Methods

Electrochemical measurements were performed using a PARSTAT 4000+ (Princeton Applied Research, Oak Ridge, TN, USA) potentiostat and a 20 A booster (KEPCO, Naju, South Korea). A two-electrode system was used. A reference electrode was not applied due to space limitations in the cell, and the object inside the bath made disturbance to the video image. Electrolysis was performed at constant cell voltage for the horizontal anode (in the interval 1.5–2.5 V) and for both anodes at constant current (in the interval 0.1–0.8 A for the horizontal anode and 0.3–6.3 A for the vertical anode). Current vs. time measurements for the horizontal anode were transformed into frequency spectra by using a Fast Fourier Transform (FFT) algorithm in "Sigview v4.3-spectrum and signal analysis" (SignalLab e.K. Pforzheim, Germany) using spectral analysis default settings. The signals were transformed into the frequency domain to evaluate how the power of the signal is distributed over a range of frequencies to determine the dominant frequency. The sampling rate (Fs) was 5 Hz. Consequently, the spectrum has a frequency range from zero to Fs/2, 0–2.5 Hz.

A two-electrode system was used, as shown in Figure 5. The working electrode is the electrode where the reaction of interests occurs, and in the present study, it was either the horizontal anode or the vertical anode. The SS rod functioned as the counter electrode. The working (WE) and working sense (WSE) connections from the potentiostat were connected to the anode, while the reference electrode (RE) and counter electrode (CE) connections were connected to a SS rod.

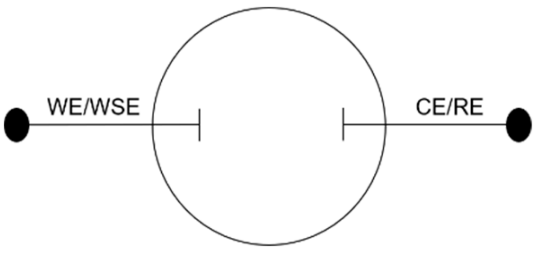

Figure 5. The schematics of the two-electrode setup, the working (WE) and working sense (WSE) connected to the anode and the counter (CE) and reference electrode (RE) connected to SS rod.

A PhotronFastcam Mini AX camera (Photron, Tokyo, Japan) was used for the video recording. Three different frame rates were used, 60 fps (frames per second) for the recording of the bubble behavior for both anode designs, and 125 and 250 fps were used in addition for the vertical anode. Recording with the higher rate was used in order to be able to capture fast events such as coalescence. Photron Fastcam Viewer 4 (PFV4) software (Photron, Tokyo, Japan) was used for controlling the Photron high-speed camera, for data saving, and for image processing. An example of the improved image quality is shown in Figure 6.

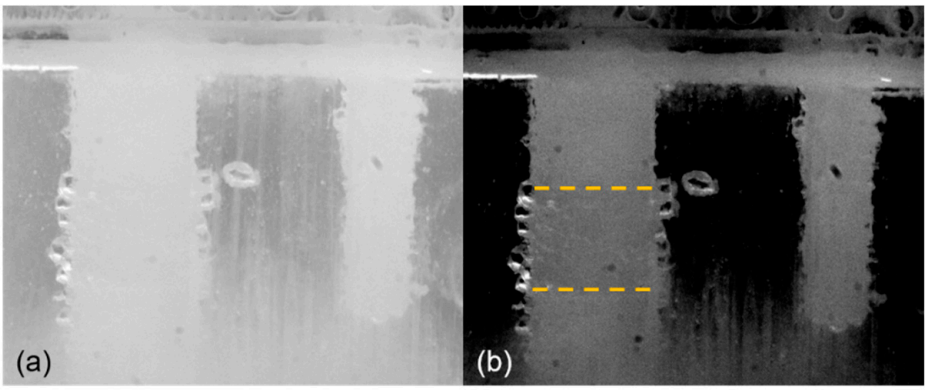

Figure 6. The image (**a**) before and (**b**) after image processing in PFV4 (Photron Fastcam Viewer 4). The image shows an example of using the vertical anode design. The yellow dashed lines indicate the border between the carbon and boron nitride material. The stainless steel rod is shown on the right in the image. The image was taken during electrolysis at a constant current density of 0.25 A cm^{-2}.

3. Results and Discussion

3.1. Bubble Behavior on the Horizontal Anode

3.1.1. Bubble Life Cycle

In Figure 7 is shown one bubble life cycle, which includes the bubble nucleation, growth, coalescence, and bubble detachment during electrolysis at a constant cell voltage of 1.5 V. The corresponding average current density was 0.4 A cm^{-2}. The beginning of the bubble cycle was defined to be when the anode surface is free of a large bubble, which is the situation right after the bubble from the previous cycle is detached, frame (1). It was found that one cycle lasts 328 frames. Since the video recording was obtained with a speed of 60 fps, the bubble cycle time was found to be 5.47 s. There was no possibility with the current setup to position the camera to observe the bottom of the horizontal anode straight from below. Therefore, the bubble nucleation and coalescence were difficult to observe. Growth of the bubbles and detachment as one big bubble was well observed from the side. The bubbles grew to a size as large or slightly larger than the horizontal carbon surface before it started to slide toward the edge (frame (325)) and was detached (frame (329)) in Figure 7.

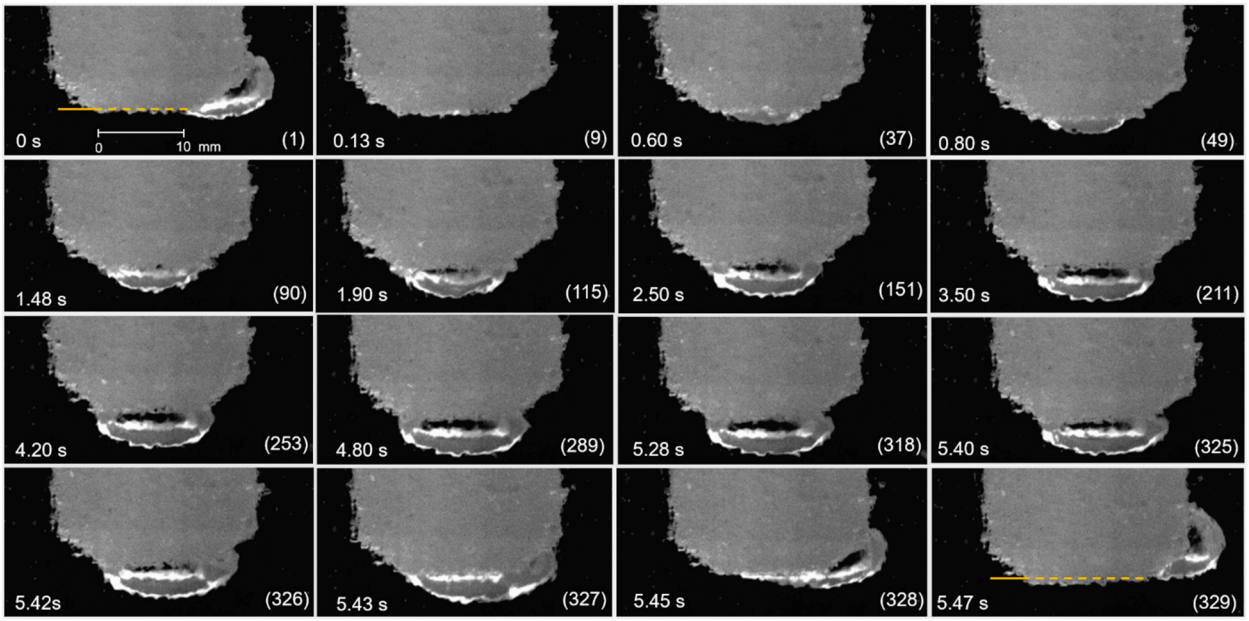

Figure 7. Cycle of one bubble at the horizontal surface during electrolysis at a constant cell voltage of 1.5 V with an average current density of 0.4 A cm^{-2}. Each individual image represents one frame with the corresponding number. The frame rate was 60 fps. The frame number is given in the brackets. Frame (1) is defined as 0 s and shows the situation right after a large bubble from the previous bubble cycle is detached from the anode surface. The horizontal yellow line in frames (1) and (329) represents the position of the carbon anode surface. A scale bar is shown in frame (1).

In Figure 8a, the details of the characteristic saw-tooth curve of the current-time data are shown. When a bubble was detached, a sharp jump in current occurred, and the current obtained its highest value. When bubbles are nucleating, growing, and coalescing, the current density decreases almost linearly while bubbles are covering more and more of the surface. At the time of detachment of a big bubble, the surface is never totally free of bubbles. As can be seen in Figure 7 for frames (1) and (329), the carbon surface is indicated with the red dashed line. While one large bubble is sliding toward the edge to be detached, the smaller bubbles are already nucleating and growing at the left part of the anode surface. From frame (329) and to a certain extent frame (1), it can be seen that the bubble layer is thicker on the left side than at the tail of the departing bubble. Bubbles strongly affect the potential components at gas-evolving electrodes. For areas where bubbles almost block the electrode surface, the current density will be close to zero, but for areas where bubbles do not block the electrode surface, the current density is greater than the average [14]. Frame (318) corresponds to the smallest current measured, i.e., when a big bubble almost covers the whole anode surface. Frame (329) corresponds to the highest current value, i.e., the time of detachment of a large bubble. From Figure 8a, the bubble cycle time was found to be around 5.5 s and is very close to 5.47 s found in Figure 7. In Figure 8b is shown the FFT analysis of current-time data, which provided a dominant frequency of 0.18 Hz corresponding to a bubble cycle time of 5.5 s. This confirms that the dominant frequency equals the bubble release frequency.

The thickness of the bubble was determined as the vertical distance between the anode surface and the bubble surface just before the bubble started to slide toward the edge of the anode for its detachment. This would correspond to frame (253) in Figure 7 for current density 0.1 A cm^{-2}. For the horizontal anode at a current density of 1 A $cm^{-2,}$ the thickness of the bubble was found to be around 4.6 mm. Most studies have suggested that the bubble layer thickness is around 5 mm in laboratory cells [8–10]. Cassayre et al. [8] observed that the bubble layer under a graphite anode (Ø 9 mm) was slightly decreasing with current density and its thickness was in the interval 4.2–5.0 mm for a current range in the interval 0.2–1.6 A cm^{-2}.

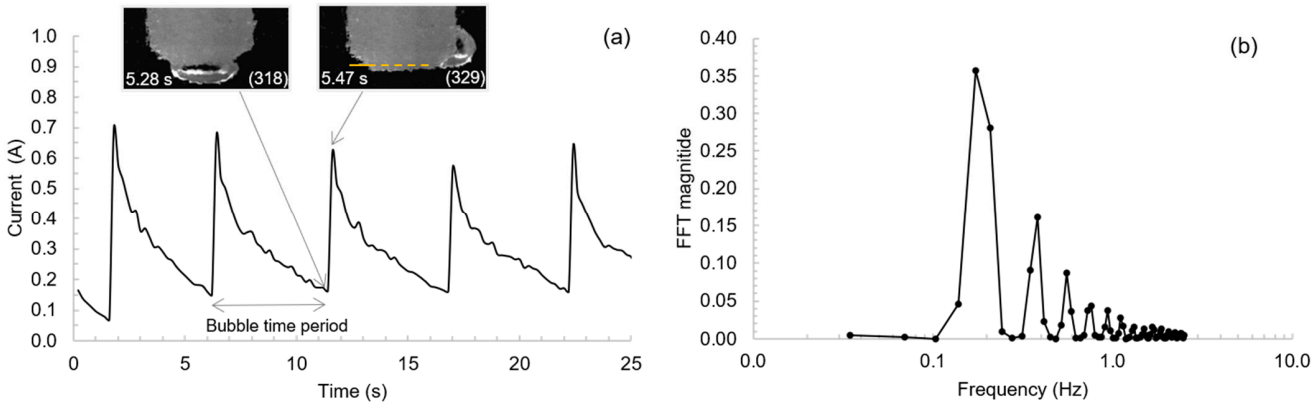

Figure 8. The horizontal anode; (**a**) current vs. time at a constant cell voltage of 1.5 V and details of the saw-tooth shaped current density-time curve. Frame (318) corresponds to the smallest current measured, and frame (329) corresponds to the current peak. (**b**) FFT (Fast Fourier Transform) spectra of current density-time data.

3.1.2. Bubble Bouncing and Bursting at the Bath Surface

In the present study, it was observed that the bubble, after its detachment from the anode surface, was rising vertically up (Figure 9) and bounced twice at the bath surface, frame (7) and frame (11), before bursting into many smaller bubbles (frame (16)). Bubble bouncing phenomena due to surface tension have also been observed in a clear water system [15] and in an air/oil/water system [19]. In the present work with cryolite bath, even not observed from the video pictures, there might have been a thin crust that the bubbles have bounced against. The superheat in the experiment was very high, around 50 °C, but also the heat loss from the furnace was largely due to the window openings. Based on this, the existence of a crust can not be excluded.

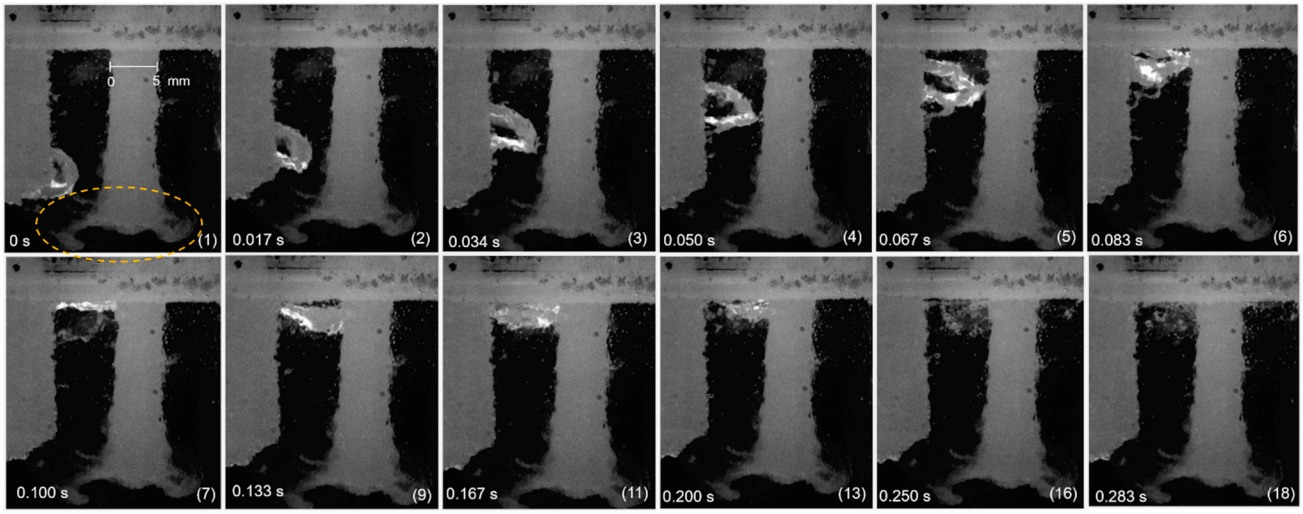

Figure 9. A bubble rising after its detachment from the horizontal surface, bouncing and bursting at the bath surface during electrolysis at a constant cell voltage of 1.5 V with the average current density of 0.4 A cm^{-2}. The frame rate was 60 fps. Frame numbers are placed in brackets. Frame (1) is defined as 0 s right after the bubble was detached from the anode surface. A scale bar is shown in frame (1).

The observed fog (highlighted at frame (1) in Figure 9) around the counter electrode (at the right) forms because the produced aluminum is not being able to dissolve in the electrolyte because the electrolyte is saturated with aluminum around the CE. Metal fog in a see-through cell has been studied by Zhuxian et al. [20].

3.1.3. Formation of Smaller Bubbles

For cell voltages above 1.8 V, it was observed that also some small bubbles detached from the surface. The average current density at 1.8 V is 0.6 A cm^{-2}. In Figure 10 is shown an example for the cell voltage equals 2.0 V, where a quite clear image was obtained. The bubble is probably nucleated at the edge of the anode, where the potential is high when the big bubble is covering the major fraction of the total anode area. The stream of smaller bubbles was also observed in the video, and the stream became more pronounced with increasing current/potential. At lower cell voltage (1.5 V), this phenomenon was not observed. This was not further investigated.

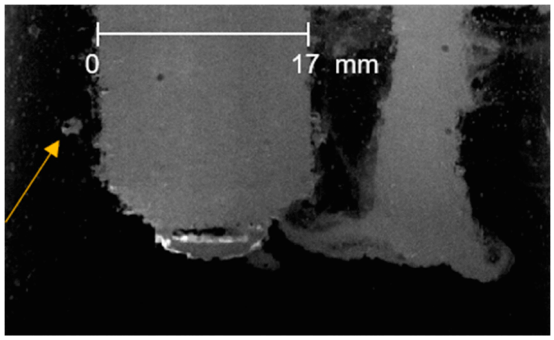

Figure 10. One small bubble detaching from the surface (yellow arrow pointing) while one large bubble growing at the surface during electrolysis at a constant cell voltage of 2.0 V. Average current density was 0.7 A cm^{-2}. A scale bar is shown.

3.1.4. Bubble Size

The average bubble diameter after bubble detachment from the horizontal surface as a function of current density is presented in Figure 11. The bubble diameter was calculated as an average value of 10 bubbles at each current density. Error bars represent a 95% confidence interval assuming a normal distribution. In Appendix A is described how the bubble diameter was measured (Figure A1). The bubble diameter decreases with increasing current density, from around 7 mm at 0.25 A cm^{-2} to around 6 mm at 1 A cm^{-2}. Cassayre et al. [8,9] measured the bubble diameter before its detachment from the surface and also found that the bubble diameter decreased with increasing current density. It was explained by less pronounced coalescence at higher current densities and that bubbles escape before covering the anode and grow to full size. An increase in current density and a corresponding increase in potential lead to an increase in the number of nucleation sites, i.e., meaning a smaller and a higher number of bubbles are formed. These bubbles coalesce into one large bubble, and the bubble cycle time is shorter. It should be added that the bubble-induced convection increases with an increasing current density as more bubbles are released from the surface. The increased convection promotes easier detachment of the bubbles and also contributes to the formation of smaller bubbles [18]. In Figure 11 is shown the bubble release frequency as a function of current density. The bubble release frequency was obtained from analysis of the recorded videos. The error bars show the 95% confidence interval. It was observed that the bubble release frequency variates (mostly increases) with the duration of the polarization, i.e., the bubble release frequency at the beginning of the polarization is lower than toward the end of the polarization. This is most pronounced at the higher current densities, 0.7 and 1.0 A cm^{-2}. This can be explained by the bubble-induced convection regime that establishes during the polarization, and convection increases with an increasing current density as more bubbles are produced and released from the anode surface and promote easier bubble removal. The FFT analysis of potential-time data was performed by using Sigview software, and dominant frequency was also obtained in Figure 11. It can be seen that the dominant frequency coincides with the bubble-released frequency. The bubble release frequency increased with increasing

current density. Going from 0.25 to 1.0 A cm^{-2}, the current density has increased by factor 4 while the bubble release frequency has increased from 0.2 to 0.5 Hz corresponding to a factor of 2.5. The difference of the factors suggests that at increasing current densities, a relatively larger amount of smaller bubbles is going off from the edge of the anode. This also was observed from the videos. The decrease in bubble diameter with increasing current density magnifies this effect.

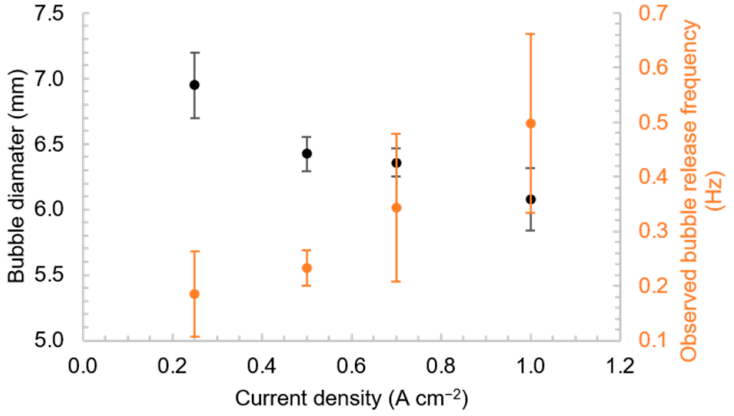

Figure 11. Bubble diameter after detachment from the horizontal surface and bubble release frequency as a function of the nominal current density.

3.1.5. Wetting of the Horizontal Anode

Solheim et al. [21] and Åsheim et al. [22] used an immersion-emersion technique to measure wetting between carbon and cryolite. It was found that the polarization strongly improved wetting for the melt low in alumina (1 wt% Al_2O_3), and the wetting increased with increased polarization. Xue and Øye [10] measured the contact angle at the horizontal anode (Ø 10 mm) in the coalescence and growth stage to be in the interval 30–45°, which was found to increase with increased bubble size. The contact angle of the bubble just before the bubble left the anode surface was measured to be 110–130°. Cassayre et al. [9] used a hot-stage microscope to study the wetting of graphite by the cryolite mixture at 1000 °C. The wetting angle on graphite was measured to be 120–130°. Huang et al. [12] used the sessile drop method to study the wettability of the cryolite at 1215 K on graphite and an industrial carbon anode and found that wettability was poor for both anodes.

In the present study, the contact angle of the bubble before it started to slide toward the edge to be detached from the horizontal anode surface was measured for different current densities. In Appendix B is shown an example of a measurement of contact angle (Figure A3). The contact angle was calculated as an average value of 4 bubbles at each current density. Error bars represent a 95% confidence interval assuming T-distribution. Results are shown in Figure 12. It was found for the horizontal anode that the average contact angle values decrease with increasing current density from 120° at 0.25 A cm^{-2} down to 105° at 1.0 A cm^{-2}. However, the error bars more or less overlap, indicating there is not a significant statistical difference. From Figure 11, it is seen that the bubble size is decreasing with increasing current density. The anode is shielded with boron nitride (BN), and according to Åsheim et al. [22], BN is better wetted by the cryolite in comparison to carbon. The big bubble could be in contact with the BN ring surrounding the anode illustrated in Figure 4b. Hence, the contact angles reported in Figure 12 could represent the contact angle in the BN/cryolite/gas system rather than for C/cryolite/gas system or a mix between them. More details on wetting and contact angles are included in the treatment of the results of the vertical anode in Section 3.2.6.

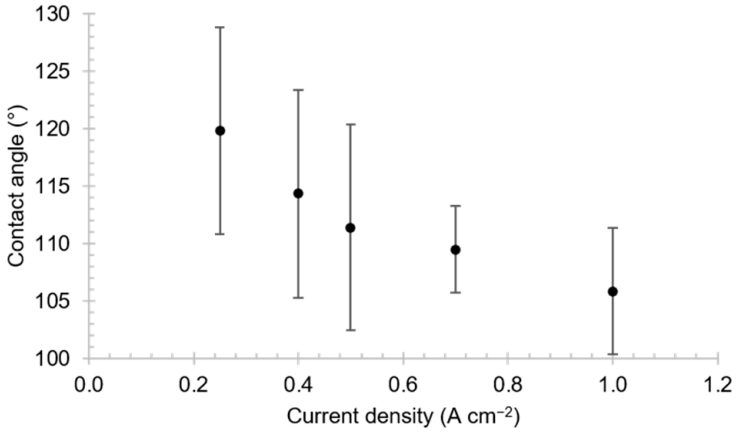

Figure 12. The change of contact angle of the bubble at the horizontal anode during electrolysis at different current densities.

3.2. Bubble Behavior on the Vertical Anode

3.2.1. Bubble Coalescence and Detachment

The bubble life cycle (nucleation, growth, coalescence, and detachment) at a vertical surface was studied in detail at low current density, 0.1 A cm^{-2}, and with higher frame rates 125 fps and 250 fps, than for the horizontal. At this current density, convection is low in comparison to higher current densities, and the transparency of the melt was at its best due to the small amount of dispersed bubbles in the melt. The images are shown in Figures 13 and 14. It was observed that the bubble formation occurred at specific nucleation sites, which was particularly evident for current densities lower than 0.5 A cm^{-2}. For higher current densities, observation is difficult due to the formation of more and smaller bubbles covering the surface. No periodic pattern in bubble growth and coalescence was found, making the bubble life cycle more of a random process. It was observed that some bubbles formed at the surface were coalescing with other bubbles, either with bubbles positioned nearby or with bubbles sliding upwards along the vertical anode surface. It was also observed that some bubbles were not coalescing, either detaching from the surface immediately or resting at the surface for a random time before detaching. In order for a bubble to leave the surface, it has to grow to a certain size. The measured diameter of detached bubbles for a current density of 0.1 A cm^{-2} was in the range of 3.3 to 3.6 mm (as discussed in Section 3.2.4). If the bubble gets entrapped at the boron nitride/carbon boundary, the resting time is radically increased, as discussed below in relation to Figure 14.

In Figure 13 is shown the process of coalescence of two bubbles into one bubble and the immediate detachment of that bubble. The upper bubble was growing at the anode surface when a smaller bubble was formed below, in frame (1). Both bubbles were growing, and the lower bubble was approaching the upper bubble. The (apparent) diameter of both bubbles was measured in frame (256) and was found to be 2.0 mm for the upper bubble and 2.5 mm for the lower bubble. The apparent bubble diameter was measured as the maximum diameter when the bubble was sticking to the surface, as shown in frame (256). In frame (257), it can be seen that the lower bubble was approaching the upper bubble. Frame (258) represents the intermediate stage in the coalescence process. In frame (259), the new bubble has obtained its final shape. The coalescence process is fast, taking place in about three frames corresponding to 0.024 s. The apparent bubble diameter after coalescence was 3.3 mm. Immediately after coalescence, the new bubble has gained enough buoyancy to be able to detach from the anode surface. The detachment process starts in frame (260). The bubble is completely detached in frame (263), and the diameter after detachment was 3.4 mm.

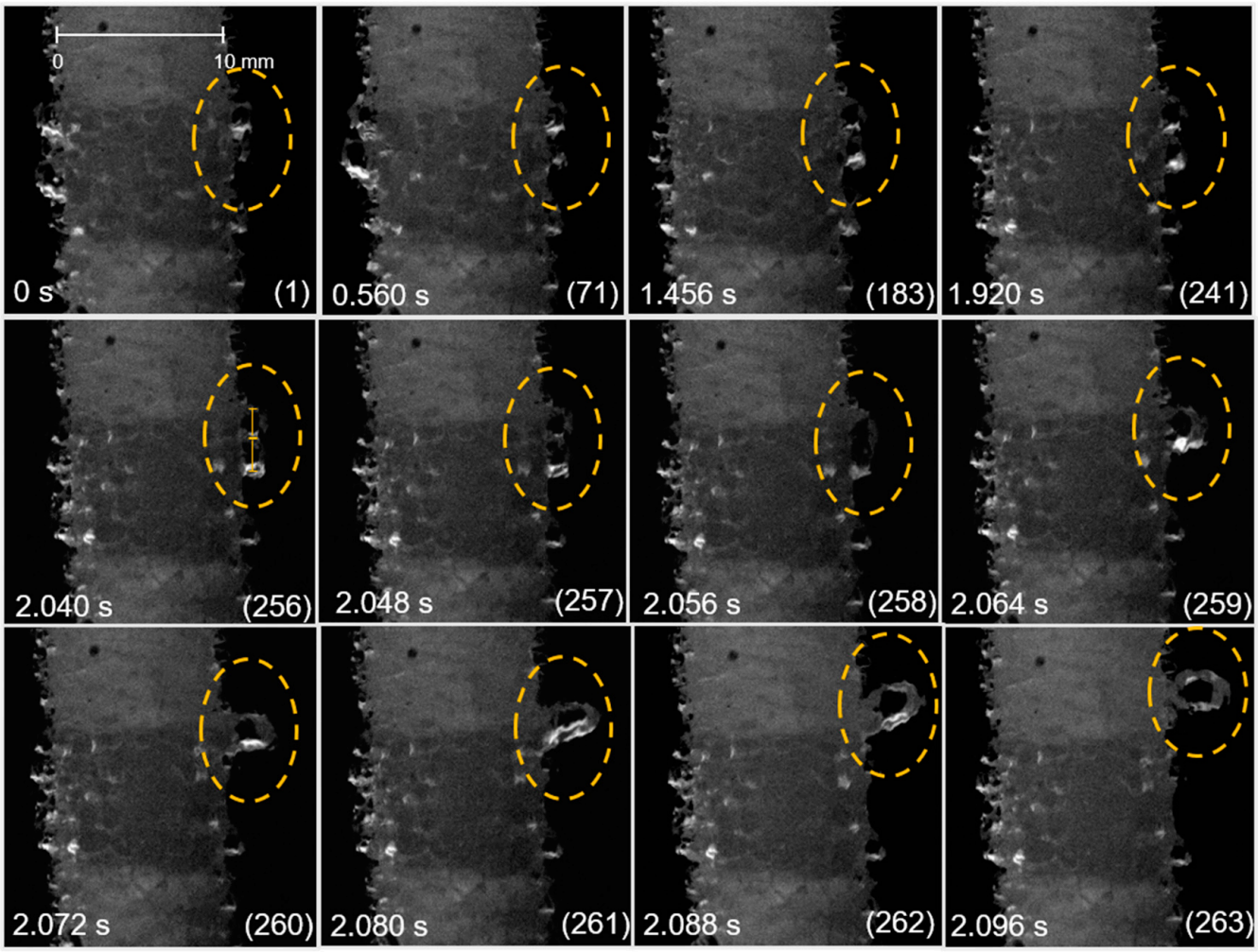

Figure 13. Process of coalescence of two bubbles (marked in yellow dashed line) into one bigger bubble and its immediate detachment from the vertical surface during electrolysis at a constant current density of 0.1 A cm^{-2}. The frame rate was 125 fps. The frame number is given in the brackets. Frame (1) is defined as 0 s. A scale bar is shown in frame (1).

In Figure 14 is shown the fast process of coalescence of three bubbles into one bubble. The diameter of the three bubbles was measured to be around 1.5 mm, frame (1). Frame (3) represents the intermediate stage in the coalescence process. In frame (4), the new bubble has obtained its shape and a diameter of 2.7 mm. The coalescence process is fast, taking place in about two frames corresponding to 0.016 s. After coalescence, the bubble was resting and growing at the boundary between boron nitride (BN) and carbon anode (C). The bubble detachment is observed in frame (295), where the bubble is rising. The bubble diameter after detachment was 3.3 mm. The long resting of the bubble at the BN/C boundary could be explained by the work of Åsheim et al. [22], who predicted that gas bubbles could be entrapped at the boundary due to better wetting of the BN by the cryolite in comparison to carbon. Probably such a bubble needs extra time to grow to a certain size because it is in contact with the BN. It probably also needs to grow bigger to be able to detach. However, no clear evidence for this was found because the size of the bubbles was in the same size range as bubbles detached from other places on the carbon surface.

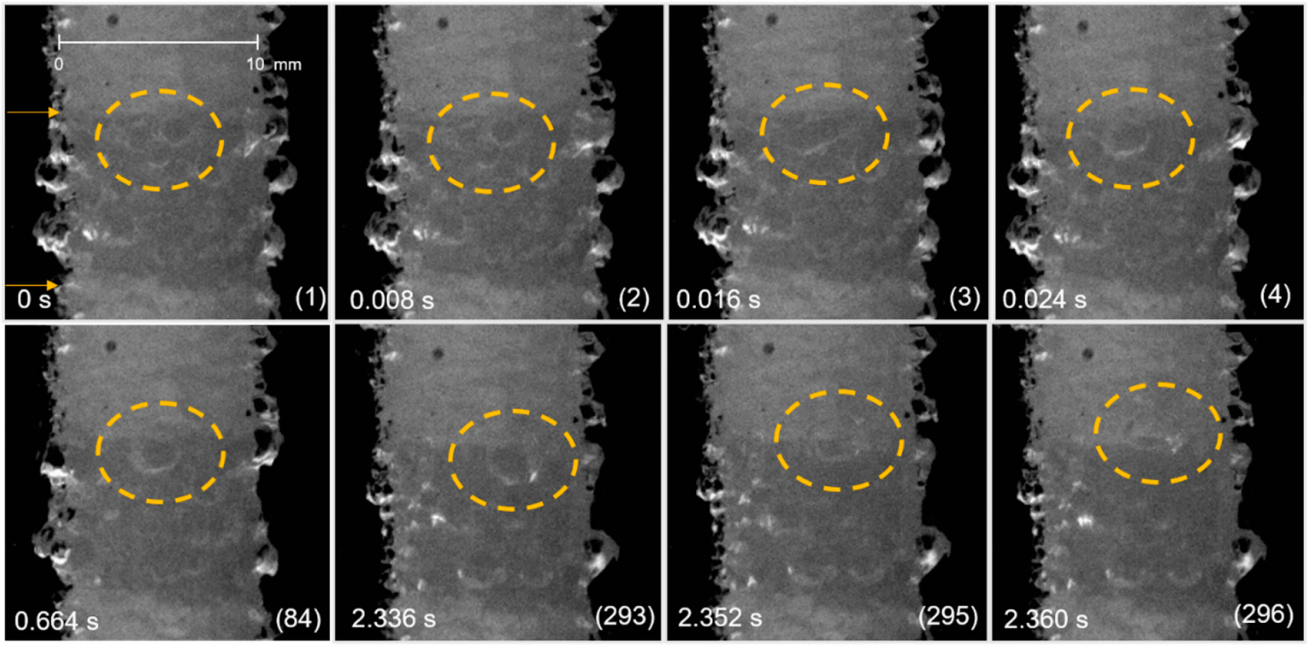

Figure 14. Process of coalescence of three bubbles (marked in yellow dashed line) into one larger bubble and its prolonged resting at the upper part of the anode at the boundary between BN and C during electrolysis at a constant current density of 0.1 A cm^{-2}. The frame rate was 125 fps. The frame number is given in the brackets. Frame (1) is defined as 0 s, indicating the start of the coalescence process. A scale bar is shown in frame (1). The yellow arrows in frame (1) indicate the C-BN borders.

The process of coalescence of bubbles at the vertical surface was also studied for three more current densities with different frame rates, 0.2 A cm^{-2} with 125 fps, 0.5 A cm^{-2} with 250 fps, and 1.0 A cm^{-2} with 250 fps. For the current density of 0.2 A cm^{-2}, the coalescence process occurred over 2 to 3 frames corresponding to 0.016–0.024 s. For the current densities of 0.5 A cm^{-2} and 1.0 A cm^{-2}, the coalescence process occurred over 4 to 5 frames corresponding to 0.016–0.020 s. For all applied current densities, 0.1, 0.2, 0.5, and 1.0 A cm^{-2}, the coalescence process took about 0.016–0.024 s, meaning the current density and electrode potential did not have a significant influence on the time for the coalescence process.

3.2.2. Bubble Bouncing and Bursting at the Bath Surface

In Figure 15 is shown an example where a bubble was hitting the bath surface three times. After detachment, the bubble is rising and hits the bath surface in frame (4), bounces and hits the bath surface again in frame (8), bounces and hits the bath surface again in frame (11) before bursting in frame (12). As discussed in relation to 3.1.2., a very thin crust could be responsible for the bubble bouncing at the bath surface.

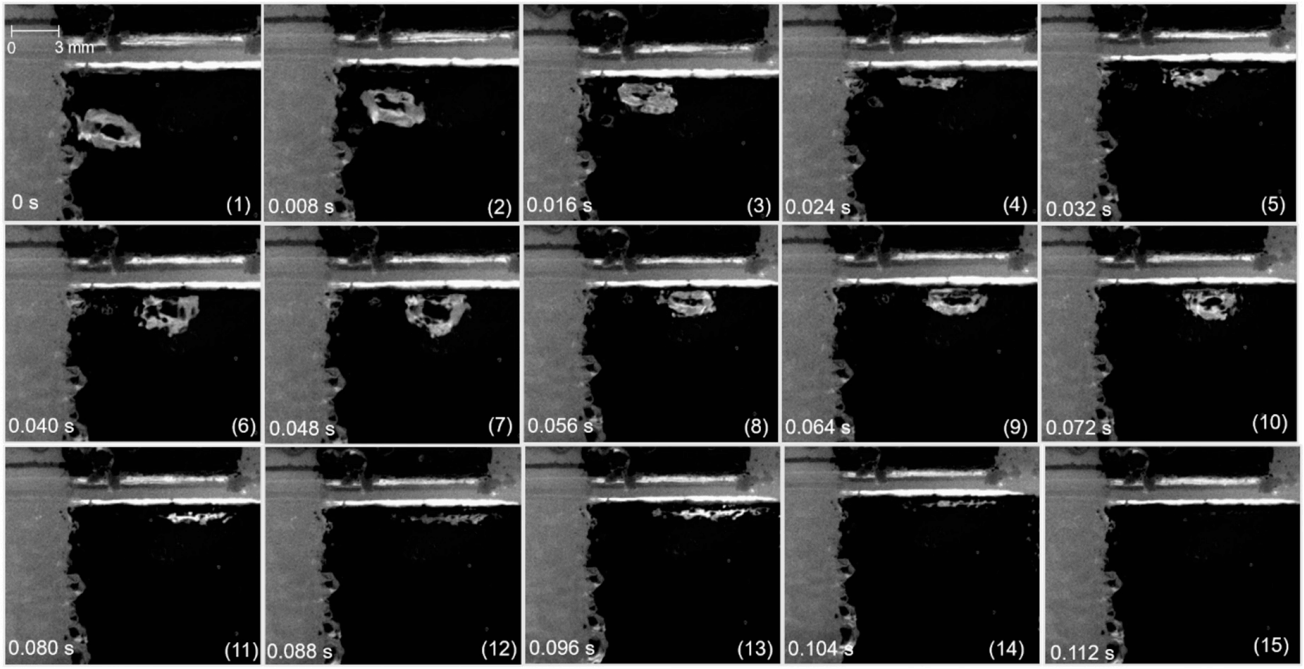

Figure 15. Bubble bouncing and bursting at the bath surface after detachment from the vertical anode at 0.1 A cm^{-2}. Upper BN part of the anode is shown. The frame number is given in the brackets. Frame (1) is defined as 0 s, indicating bubble detachment from the carbon surface and rise. A scale bar is shown in frame (1).

3.2.3. Formation of Smaller Bubbles

During the bubble life cycle, it was found that also some smaller bubbles (Ø ~ 1 mm) were detached from the surface, although not many bubbles (Figure 16). With the increasing current density, this phenomenon became more pronounced. At the stainless steel rod (to the right) it could be observed a droplet at the rod bottom, which probably is aluminum produced.

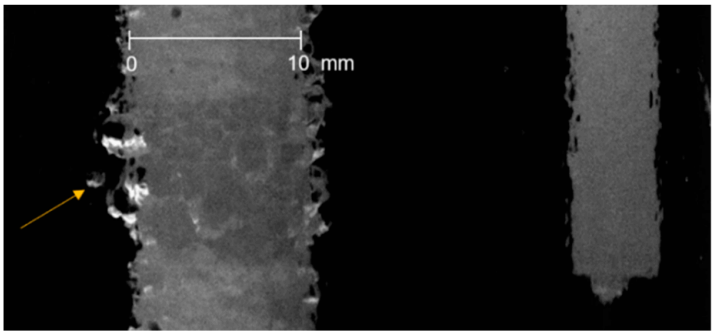

Figure 16. One small bubble (yellow arrow pointing) is detaching from the vertical surface (at the left) at a constant current density of 0.1 A cm^{-2}. A scale bar is shown in the figure.

3.2.4. Bubble Size

The average bubble diameter after detachment from the vertical surface as a function of current density is presented in Figure 17. It was calculated as an average value of 10 bubbles at each current density. Error bars represent a 95% confidence interval assuming a normal distribution. In Appendix A is described how the bubble diameter was measured (Figure A2). The bubble diameter is decreasing with increasing current density, from around 3.4 mm at 0.1 A cm^{-2} to around 1.7 mm at 2.0 A cm^{-2}. The increase in current density and thereby the corresponding increase in potential provide a higher driving force for nucleation of relatively more bubbles. The bubble-induced convection is more efficient

for the vertical anode than for the horizontal anode due to the increased number and smaller bubbles formed on the vertical anode. The larger flow makes bubble detachment faster. The buoyancy also favors the vertical since for the horizontal anode, the bubbles have to grow to a larger in size before being able to detach.

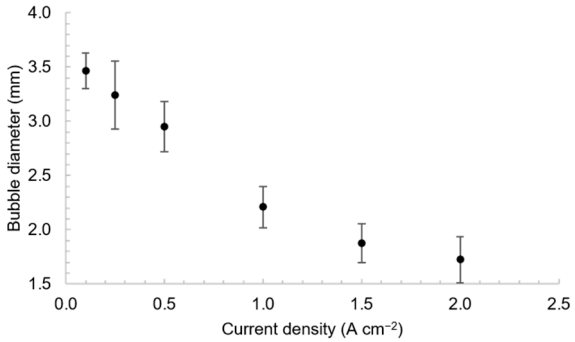

Figure 17. Bubble diameter after detachment from the vertical surface as a function of nominal current density.

3.2.5. Bubble Dynamics at Different Current Densities

In Figure 18 can be seen bubble evolution at different current densities: 0.1, 0.5, 1.0, and 1.5 A cm^{-2}. With increased current density, more and smaller bubbles are released from the anode surface. At 1.5 A $cm^{-2,}$ it is difficult to distinguish the carbon from the BN due to the great amount of smaller bubbles that hinder visibility. At the counter electrode, aluminum is produced, and in Figure 18c for 1.0 A $cm^{-2,}$ it is evident that aluminum fog is approaching the anode. At 1.5 A cm^{-2} in Figure 18d, the melt is less transparent because of more fog produced and more efficient spread from convection in addition to more numerous and smaller bubbles.

3.2.6. Wetting of the Vertical Anode

In the present work, contact angles of bubbles at the vertical anode were measured for different current densities, 0.1, 0.5, and 1.0 A cm^{-2}. Angles were measured for bubbles in two different stages in the bubble cycle, i.e., in the growth stage before coalescence and after coalescence just before detachment from the surface. An example of how the contact angle was measured is shown in Figure A4 in Appendix B. If the bubble was moving very slowly, i.e., sliding upwards along the surface, the advancing and receding contact angles could be measured. The bubbles were, to a small degree, observed sliding up along the carbon surface. The bubbles measured were either resting at the surface or in the detachment process. The measured contact angles were therefore termed as lower and upper rather than advancing and receding contact angles, respectively. The measured contact angles of bubbles and corresponding bubble diameter are shown in Figure 19 as a function of current density. Contact angles were calculated as an average value of 4 bubbles at each current density. Error bars are in 95% confidence interval assuming T-distribution. As mentioned earlier, Åsheim et al. [22] found that the wetting is improved with the increased polarization, i.e., increased current density. In the present paper, it was not observed a decrease in contact angle with an increase in current density, which would indicate improvement in wetting. Only slight variations in contact angle were observed, which could depend more on bubble size than polarization.

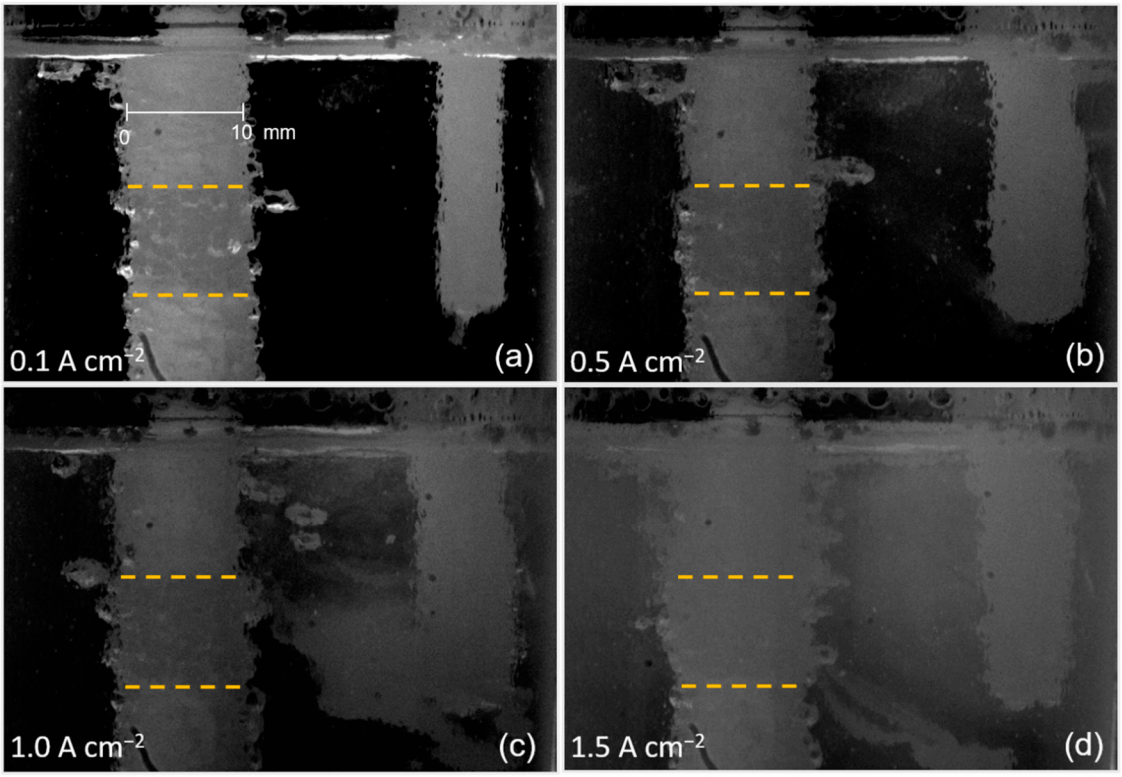

Figure 18. Images of bubble evolution at the vertical anode during electrolysis at different current densities: (**a**) 0.1, (**b**) 0.5, (**c**) 1.0, and (**d**) 1.5 A cm^{-2}. The yellow line indicates the border between the carbon and boron nitride material. The frame rate was 125 fps. A scale bar is shown in (**a**).

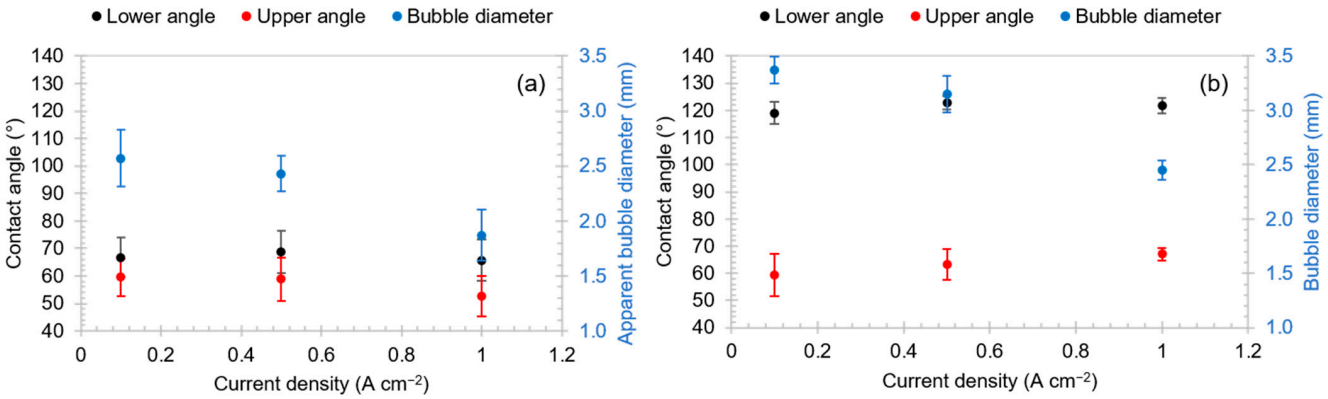

Figure 19. Lower and upper contact angle and the bubble diameter as a function of applied current density for the vertical anode, (**a**) for the bubble resting at the surface in the growth stage just before coalescence (**b**) for the bubble after coalescence just before detachment.

The modified Young equation describes the relationship between the cosine of the contact angle and the base radius of the drop (bubble) [23,24]:

$$\cos\theta = \cos\theta_{\infty} - \frac{\gamma_{slg}}{r \cdot \gamma_{lg}} \quad (5)$$

θ is the contact angle, θ_{∞} when $r \rightarrow \infty$, r is the drop (bubble) base radius.

According to the modified Young equation Equation (5), a decrease in bubble diameter should increase the wetting angle, i.e., the wetting decreases. Applied to Figure 19, this

indicates that the increase in wetting expected from an increase in polarization might be counteracted by a decrease in the bubble size with current density.

For the bubbles resting at the vertical surface in the growth stage just before coalescing with other bubbles, the lower angle was measured to be around 67°, and it seems not to vary significantly with the increased in current density, Figure 19a. The apparent bubble diameter was measured as the maximum diameter when the bubble was sticking to the surface, as shown in Figure 13 (frame 256). The upper angle was measured to be around 55°, and it seems to slightly decrease with the increasing current density, Figure 19a. An increase in current density is accompanied by a decrease in bubble size, as shown in Figure 17. Hence contact angle slightly increases with the increase in bubble size.

Drelich et al. [23,25] studied advancing and receding contact angle for water and ethylene glycol and the air bubble and water system for a homogenous surface and different heterogeneous surfaces as a function of a drop (bubble) size. For the smooth and homogeneous surface, Drelich observed that both advancing and receding angles remained constant with small variations (~3°) for the system with a 1–7 mm drop (bubble) diameter. For rough and heterogeneous surfaces, only a slight variation in the advancing contact angle value occurred while receding contact angles measured with the use of the sessile drop technique decreased with the drop or bubble size for all examined rough surfaces. Drelich concluded that surface roughness and heterogeneity affect the contact angle and drop or bubble size relationship for the system with 1–7 mm drop or bubble diameter. In the present work, the upper angle, which corresponds to the receding angle, seems to slightly, although not significantly, increase with the increasing bubble diameter. The bubble diameter interval is narrow, less than 1 mm, which is probably not large enough to see a bigger picture and to relate Drelich's conclusions with the obtained results.

In the final stage of the bubble cycle, just before its detachment from the anode surface, the lower and upper contact angles also showed little variation with the increase in current density, as shown in Figure 19b. The lower contact angle is measured to be around 120° and the upper around 67°. The values of the upper angles increased from ~55° to ~67°, from (a) to (b) but values for the lower angle increased significantly: from ~67° to ~120°. The difference between measured upper and lower contact angles from Figure 19a,b is mainly due to different stages in the bubble life cycle and different bubbles state (static/dynamic). Bubbles in Figure 19a are sticking at the surface and are in the growth stage just before coalescence. After coalescence, the bubbles have grown large enough to be detached from the surface Figure 19b. Measured contact angles in Figure 19a are considered to be static because the bubble is sticking to the surface; the lower contact angle is slightly higher than the upper contact angle due to the buoyancy effect, which acts on the bubble at the vertical surface. For bubbles in Figure 19b, the detachment process has already started as the detachment process started immediately after the coalescence. In general, a contact angle for a bubble in a detachment process is considered to be dynamic [26]. The bubble undergoes deformation, and the apparent symmetrical shape of the bubble was distorted. Hence, the lower contact angle increased significantly in going from (a) to (b).

With the increased polarization, only slight variations in contact angle were observed. According to Åsheim et al. [22], wetting is improved with the increased polarization. For the present work, the alumina saturation was around 3.4 wt% at 898 °C according to calculation obtained by Software for Aluminum Smelting [27]. Since the alumina concentration was 3 wt%, the bath is close to saturation. Solheim et al. [21] observed in a bath with high alumina concentration (8 wt%) that polarization did not affect wetting significantly since the increase in alumina concentration changed the wetting of carbon by cryolite from non-wetting to good wetting. However, the actual alumina concentration might be as important as the degree of saturation. The alumina concentration of 3 wt% in the present work is probably lower than the concentration needed to make the wetting change from non-wetting to good wetting. Fellner and Lubyova [28] studied the influence of the addition of different additives, among others LiF, on the wetting of graphite by cryolite. It was concluded that in an acidic bath, LiF has no effect on wetting, while in

neutral and basic baths, LiF increases contact angle. In the present work, the bath contained 15 wt% LiF, 15 wt% AlF_3, and 5 wt% of CaF_2. The bath could therefore be neutral or slightly basic, and it is difficult to judge the influence of LiF on the actual contact values. However, the trends should be unaffected.

3.3. Impact of Results and Relation to Other Works

3.3.1. Small Laboratory-Scale Anodes

One of the aims of the present work was to gain more knowledge for further improvement of the laboratory-scale studies. Based on the obtained results, the following could be stated:

1. Position of the counter electrode (CE): The current distribution across the working electrode (WE) is important. The CE was placed to the right of the WE, meaning the current path to the left side of the WE is longer than for the right side. During all experiments, it was not observed more bubbles forming on the right side of the WE compared to the left side. It can then be assumed that the current distribution for this electrode setup is sufficiently suitable for all practical purposes. This supports the findings in the work of Stanic et al. [18].
2. Bubbles resting at the BN surface: During all experiments, bubbles were observed resting at the boron nitride surfaces. The bubbles were formed as soon as the anode was immersed in the melt. The bubbles did not take part in any electrochemical reaction, and the same bubbles rested at the surface during the entire experiment, which typically could last about one hour for one specific electrode. The bubbles are thought to be either moisture or nitrogen arising from the bulk of the BN material.
3. Bubbles resting at the carbon surface: When immersing the anode in the melt, it was observed that bubbles to some degree formed at the carbon surface before any current or potential were applied. The phenomenon was most pronounced for the horizontal anode where one big bubble was formed at the surface and interfered with the experiment. By gently vibrating the anode, the bubble could be removed but a new bubble formed in less than one minute. In the timeframe before a new bubble formed, the electrochemical measurement could be started. The bubble formation caused potential overloading of the potentiostat when using the horizontal anode because the large bubble covered almost the whole anode surface.

The origin of the bubbles formed at both carbon and BN surfaces is not identified, although humidity and nitrogen gas are two compounds that are suspected. The anodes were dried at 120 °C for two to three hours before introduced to the cell. Even after having been immersed in the melt at 890 °C for one hour, the bubbles still formed. However, the bubbles are believed not to interfere with the electrochemical experiments because the bubbles on the carbon were easily displaced by the electrochemically formed CO and CO_2. For experiments involving gas coverage and gravimetric measurements, one should pay attention to the existence of these bubbles, e.g., Åsheim et al., where wetting of carbon anodes with and without BN shielding was studied by a gravimetric anode.

4. Presence of metal fog: The presence of fog can influence bubble size, wetting, reaction products. Metal fog can be electrochemically oxidized on the anode, and the CO/CO_2 ratio can be changed by the back reaction. Figure 18 shows that more fog is produced at higher current densities. For cathodic current densities up to 0.05 A cm^{-2} (the corresponding anodic current density is then about 0.1 A cm^{-2} as the counter electrode has approximately twice the area of the vertical anode), the fog does not reach the anode in the time frame of the recording, which lasted about 40 s. For cathodic current densities around 0.25 A $cm^{-2,}$ the fog reached the anode after 20 s. At higher current density, this time decreased. To reduce complications caused by the metal fog, the anode and cathode should be physically separated at least for longer duration experiments. Examples for physical separation can be found in the work by Zhao et al. [11], Stanic et al. [29], and Silny and Utigard [30]. A pool of aluminum at the bottom of the crucible could help by having a less foggy electrolyte.

3.3.2. Laboratory-Scale Anodes Versus Industrial Anodes

For the lab anodes, it was found that with increasing current density, more and smaller bubbles formed at the surface as the increase in potential causes the number of nucleation sites to increase. The bubble release frequency was found to slightly increase with the duration of the polarization, and the size of released bubbles was observed to decrease. Overall the increased number of smaller bubbles screen the anode surface to a higher degree. Kiss et al. [31] developed a mathematical model of the bubble layer in an aluminum reduction cell based on microscopic modeling. From simulations, it was found that (when the size of the anode is large enough) big gas bubbles move slowly toward the edge of the anode and sweep away smaller bubbles during their movement. Instead of having many smaller bubbles detaching randomly, the detachment of the gas is more organized with bigger bubbles. A larger bubble gives a higher probability for collision with other bubbles. Wang et al. [32] concluded that the anode size has some influence on the bubble size. Horizontal anodes with 20, 30, and 40 mm in diameter were studied. The bubble size was found to decrease with decreasing surface area for the same current density. Einarsrud [33] carried out experiments on an industrial cell and found that with increasing anode age, the voltage oscillation related to bubbles increased in frequency and in magnitude due to the slots worn down toward the end of the anode service time. The disappearing of the slots makes in practice a larger anode and probably reflects the same phenomenon, i.e., larger bubbles with increased anode size both for lab and industrial-sized anodes illustrating some similar findings at different scales. Wang and Taberaux [34] studied gas bubbling using an intermediate size anode (15.2 cm in diameter) and the impact of anode consumption. The electrolysis was conducted at 200 A for over 72 h. For an anode with a large diameter and sharp edges, the bubble volume increased as current density increased till it reached a maximum (at ~0.8 A cm^{-2}) and then decreased with a further increase in current density. For an anode with reduced diameter and rounded edge, an increase in current density increased both bubble frequency and bubble volume, although the bubble size was always smaller than for the anode with sharp edges. In the present paper using a small lab anode (10 mm in diameter), it was observed that the size of the detached bubble decreased with increasing current density, which can be comparable with the results of Wang and Taberaux for the sharp edge anode after a reaching specific current density. The increased current density causes larger bubble-induced convection, which might be the main cause of the observed trends. The bubble size obtained with the rounded edge anode of Wang and Taberaux is probably less influenced by the current induced convection and does not have an initial high bubble size or a maximum bubble size.

4. Conclusions

At the horizontal downward-facing surface, the bubbles grew and coalesced to form one large bubble that then grew larger and finally started to slide toward the edge of the anode surface for detachment. Even though the big bubble detached, the surface was never free of bubbles for the studied current density range 0.25–1.0 A cm^{-2}.

At the vertical anode surface, the detaching bubbles were smaller, and most of them had been going through a coalescence process prior to detachment. Coalescence of two and three bubbles into one bigger bubble was observed on the vertical anode surface. The coalescence process occurred quite fast, in the interval 0.016–0.024 s from initiation to the final bubble shape was established. Some intermediate stages in the coalescence process were captured.

The bubble diameter decreased with the increasing current density for both the horizontal and the vertical anode. Explanations for these observations are the larger number of nuclei formed at higher potential and the more efficient bubble-induced convection.

The measured contact angles for the vertical anode termed as lower and upper contact angles showed little variation with change in current density. It was assumed that the current density had a stronger effect on the contact angle through its effect on the bubble size than the polarization and associated surface roughening. The applied current densities

(0.1–1.0 A cm^{-2}) and the obtained bubble diameter interval (~ 1.9–2.6 mm) were probably not large enough to reveal eventual changes in the contact angle.

The obtained results are helpful for easier and better design of laboratory-scale studies investigating, e.g., current distribution, anode bubble evolution, current efficiency, and wetting properties.

Author Contributions: N.S. performed all the experimental work and wrote the manuscript with input from E.S., K.E.E., and A.M.M., E.S. supervised the work. All authors have read and agreed to the published version of the manuscript.

Funding: This research was funded by the Norwegian University of Science and Technology. The APC was funded by the Norwegian University of Science and Technology.

Institutional Review Board Statement: Not applicable.

Informed Consent Statement: Not applicable.

Data Availability Statement: Not applicable.

Conflicts of Interest: The authors declare no conflict of interest.

Appendix A

Bubble diameter was measured based on the pixel information using PFV4 software. The target bubble was a bubble detached from the carbon surface and had a nearly spherical shape. In Figures A1 and A2 are shown examples of some nearly spherical-shaped bubbles during electrolysis for the horizontal and the vertical anode, respectively. The diameter was measured as shown in Figures A1 and A2 and was defined as the distance between two points of the spherical bubble.

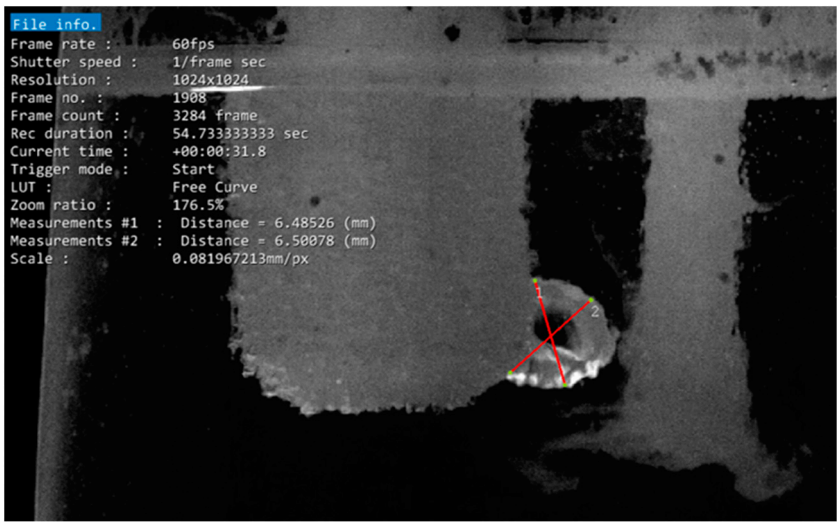

Figure A1. An example of measurement of the bubble diameter during electrolysis using the horizontal anode at current density 0.7 A cm^{-2}. The average value was used.

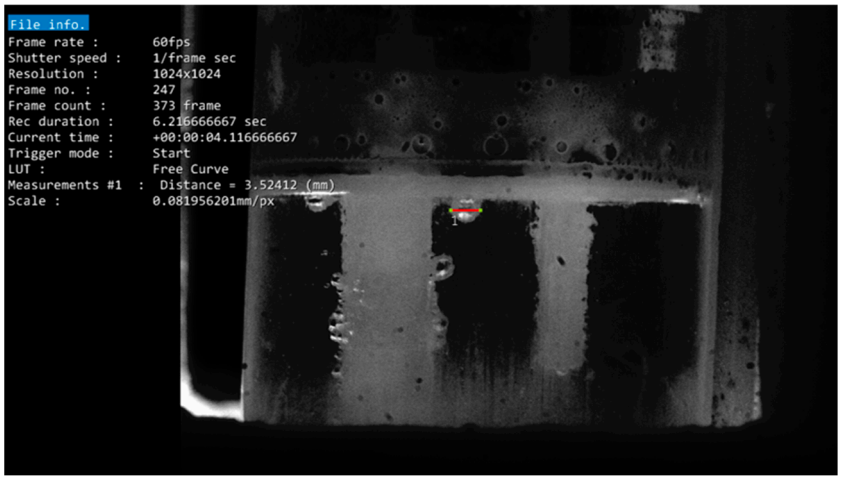

Figure A2. An example of measurement of the bubble diameter during electrolysis using the vertical anode at current density 0.25 A cm^{-2}.

Appendix B

The contact angle of the bubble at the horizontal and vertical anode was measured by drawing a tangent to the bubble profile at the point of the three-phase contact on an enlarged image. An example of a measurement of contact angle for the horizontal anode is shown in Figure A3, and an example for lower and upper contact angle for the vertical anode just before detachment is shown in Figure A4.

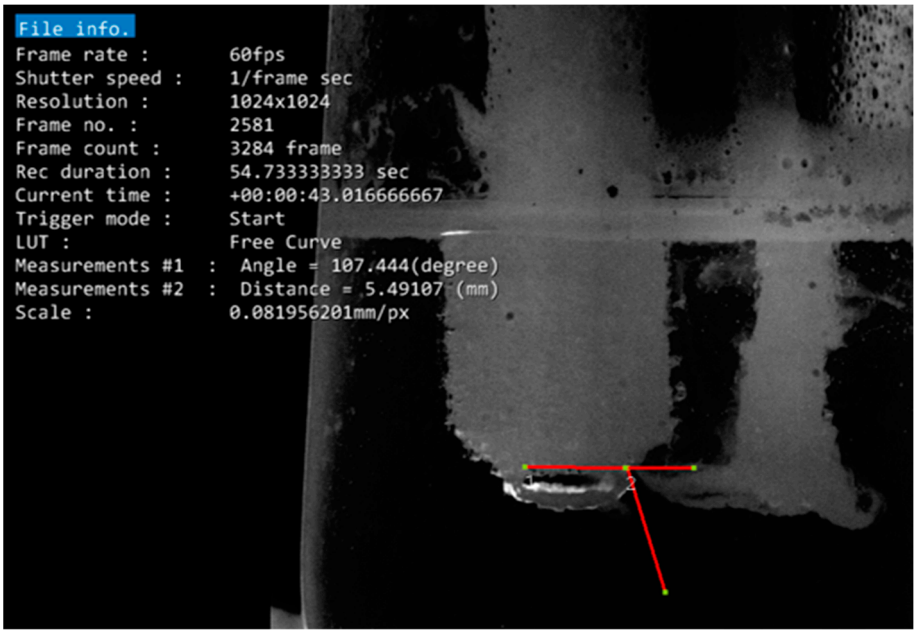

Figure A3. An example of measurement of wetting angle of the bubble on the horizontal anode just before it started to slide toward the edge of the anode to be detached during electrolysis at an average current density of 0.7 A cm^{-2}.

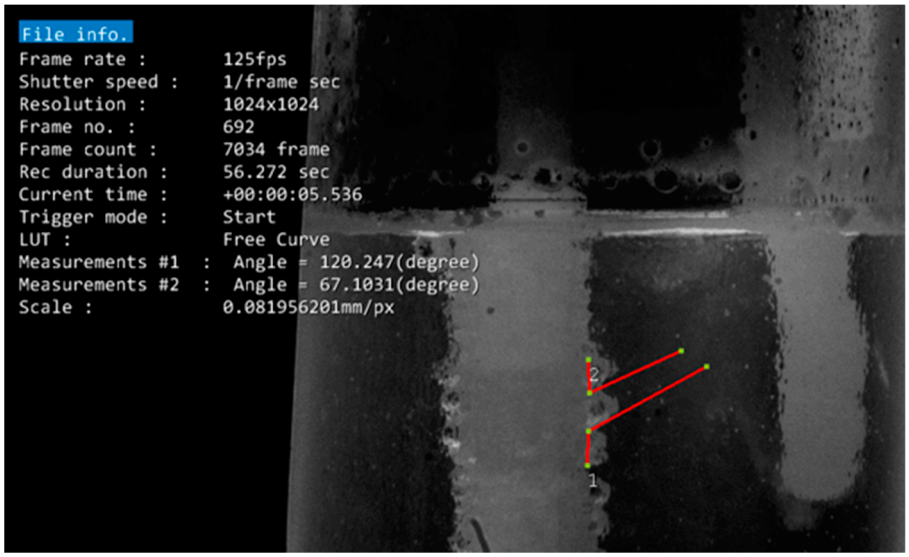

Figure A4. An example of measurement of lower and upper contact angle of the bubble just before detachment on the vertical anode during electrolysis at a constant current density of 0.5 A cm^{-2}.

References

1. Grjotheim, K.; Kvande, H. *Introduction to Aluminium Electrolysis: Understanding the Hall-Héroult Process*, 2nd ed.; Aluminium-Verlag: Düsseldorf, Germany, 1993; pp. 1–9, 43–45, 50–60, 119–127.
2. Thonstad, J.; Fellner, P.; Haarberg, G.M.; Híveš, J.; Kvande, H.; Sterten, Å. The Anode Process. In *Aluminium Electrolysis: Fundamentals of the Hall-Héroult process*, 3rd ed.; Aluminium-Verlag: Düsseldorf, Germany, 2001; pp. 158–215.
3. Tabereaux, A.T.; Peterson, R.D. Aluminum Production. In *Treatise on Process Metallurgy*, 1st ed.; Seetharaman, S., Ed.; Elsevier: Boston, MA, USA, 2014; pp. 839–917.
4. Zhao, Z.; Wang, Z.; Gao, B.; Feng, Y.; Shi, Z.; Hu, X. Observation of Anodic Bubble Behavior Using Laboratory Scale Transparent Aluminium Electrolysis Cells. In *Light Metals 2015*; Hyland, M., Ed.; Springer: Berlin, Germany, 2015; pp. 801–806.
5. Hyde, T.M.; Welch, B.J. The Gas Under Anodes in Aluminium Smelting Cells. Part I: Measuring and Modelling Bubble Resistance under Horizontally Oriented Electrodes. In *Light Metals*; TMS: Pittsburgh, PA, USA, 1997; pp. 333–341.
6. Haupin, W. Interpreting the components of cell voltage. In *Light Metals 1998*; TMS: Pittsburgh, PA, USA, 1998; pp. 531–537.
7. Einarsrud, K.E.; Eick, I.; Bai, W.; Feng, Y.; Hua, J.; Witt, P.J. Towards a coupled multi-scale, multi-physics simulation framework for aluminium electrolysis. *Appl. Math. Model* **2017**, *44*, 3–24. [CrossRef]
8. Cassayre, L.; Plascencia, G.; Marin, T.; Fan, S.; Utigard, T. Gas Evolution on Graphite and Oxygen-Evolving Anodes During Aluminium Electrolysis. In *Light Metals 2006*; Galloway, T.J., Ed.; TMS: Pittsburgh, PA, USA, 1995; pp. 379–383.
9. Cassayre, L.; Utigard, T.; Bouvet, S. Visualizing gas evolution on graphite and oxygen-evolving anodes. *JOM* **2002**, *54*, 41–45. [CrossRef]
10. Xue, J.; Øye, H.A. Bubble behaviour: Cell voltage oscillation during aluminium electrolysis and the effects of sound and ultrasound. In *Light Metals 1995*; Evans, J., Ed.; TMS: Pittsburgh, PA, USA, 1995; pp. 265–271.
11. Zhao, Z.; Wang, Z.; Gao, B.; Feng, Y.; Shi, Z.; Hu, X. Anodic Bubble Behavior and Voltage Drop in a Laboratory Transparent Aluminum Electrolytic Cell. *Metall. Mater. Trans. B* **2016**, *47*, 1962–1975. [CrossRef]
12. Huang, Y.; Wang, Z.; Yang, Y.; Gao, B.; Shi, Z.; Hu, X. Anodic Bubble Behavior in a Laboratory Scale Transparent Electrolytic Cell for Aluminum Electrolysis. *Metals* **2018**, *8*, 806. [CrossRef]
13. Kiss, L.; Poncsak, S.; Toulouse, D.; Perron, A.; Dröge, A.; Mackowiak, V. Detachment of bubbles from their nucleation sites. In *Multiphase Phenomena and Cfd Modeling and Simulation in Materials Processes*; TMS: Pittsburgh, PA, USA, 2004; pp. 159–168.
14. Haberman, W.L.; Morton, R.K. *An Experimental Investigation of the Drag and Shape of Air Bubbles Rising in Various Liquids*; Report 802 NS 715-102, Techincal Report for Navy Department; The David W. Taylor Model Basin: Washington, DC, USA, 1953; Volume 15.
15. Zawala, J.; Dorbolo, S.; Vandewalle, N.; Malysa, K. Bubble bouncing at a clean water surface. *Phys. Chem.* **2013**, *15*, 17324–17332. [CrossRef] [PubMed]
16. Manica, R.; Klaseboer, E.; Chan, D. The impact and bounce of air bubbles at a flat fluid interface. *Soft Matter* **2016**, *12*, 3271–3282. [CrossRef] [PubMed]
17. Haupin, W. The Liquidus Enigma. In *Light Metals 1992: Proceedings of the Technical Sessions Presented by the TMS Light Metals Committee at the 121st TMS Annual Meeting, San Diego, CA, USA, 1–5 March 1992*; Cutshalled, E.R., Ed.; Minerals, Metals & Materials Society: Pittsburgh, PA, USA, 1991; pp. 477–480.

18. Stanic, N.; Jevremovic, I.; Martinez, A.M.; Sandnes, E. Bubble Evolution on Different Carbon Anode Designs in Cryolite Melt. *Metall. Mater. Trans. B* **2020**, *51*, 1243–1253. [CrossRef]
19. Feng, J.; Muradoglu, M.; Kim, H.; Ault, J.T.; Stone, H.A. Dynamics of a bubble bouncing at a liquid/liquid/gas interface. *J. Fluid Mech.* **2016**, *807*, 324–352. [CrossRef]
20. Zhuxian, Q.; Liman, F.; Grjotheim, K.; Kvande, H. Formation of metal fog during molten salt electrolysis observed in a see-through cell. *J. Appl. Electrochem.* **1987**, *17*, 707–714. [CrossRef]
21. Solheim, A.; Gudbrandsen, H.; Martinez, A.M.; Einarsrud, K.E.; Eick, I. Wetting between Carbon and Cryolitic Melts. Part II: Effect of Bath Properties and Polarisation. In *Light Metals 2015*; John Wiley & Sons, Inc.: Hoboken, NJ, USA, 2015; pp. 671–676.
22. Åsheim, H.; Eidsvaag, I.A.; Solheim, A.; Gudbrandsen, H.; Haarberg, G.M.; Sandnes, E. The Influence of Polarisation on the Wetting of Graphite in Cryolite-Alumina Melts. In *Light Metals 2020*; Springer International Publishing: Berlin, Germany, 2020; pp. 608–619.
23. Drelich, J. The Effect of Drop (Bubble) Size on Contact Angle at Solid Surfaces. *J. Adhes.* **1997**, *63*, 31–51. [CrossRef]
24. Boruvka, L.; Neumann, A.W. Generalization of the classical theory of capillarity. *J. Chem. Phys.* **1977**, *66*, 5464–5476. [CrossRef]
25. Drelich, J.; Miller, J.D.; Good, R.J. The Effect of Drop (Bubble) Size on Advancing and Receding Contact Angles for Heterogeneous and Rough Solid Surfaces as Observed with Sessile-Drop and Captive-Bubble Techniques. *J. Colloid Interface Sci.* **1996**, *179*, 37–50. [CrossRef]
26. Wang, G.; Feng, D.; Nguyen, A.; Evans, G.M. The dynamic contact angle of a bubble with an immersed-in-water particle and its implications for bubble–particle detachment. *Int. J. Miner. Process.* **2016**, *151*, 22–32. [CrossRef]
27. Software for Aluminum Smelting. 2005. Available online: https://peter-entner.com/E/ElProp-2/ElProp-2.htm (accessed on 20 December 2020).
28. Fellner, P.; Lubyova, Ž. Influence of LiF, CaF_2, MgF_2 additives and of dissolved aluminium on wetting of graphite by the cryolite-based melt. *Chem. Papers* **1991**, *45*, 201–204.
29. Stanic, N.; Bø, E.T.; Sandnes, E. CO and CO_2 Anode Gas Concentration at Lower Current Densities in Cryolite Melt. *Metals* **2020**, *10*, 1694. [CrossRef]
30. Silny, A.; Utigard, T.A. Determination of the factors which control the CO/CO_2 ratio of the anode gas. In *Light metals 1995*; Evans, J.W., Ed.; Minerals, Metals & Materials Society: Pittsburgh, PA, USA, 1995; pp. 205–211.
31. Kiss, L.I.; Poncsak, S.; Antille, J. Simulation of the Bubble Layer in Aluminium Electrolysis Cells. In *Light Metals 2005*; Kvande, H., Ed.; TMS: Pittsburgh, PA, USA, 2005; pp. 559–564.
32. Wang, Z.; Gao, B.; Li, H.; Shi, Z.; Lu, X.; Qiu, Z. Study on Bubble Behavior on Anode in Aluminum Electrolysis-Part I. In *Light Metals 2006: Proceedings of the Technical Sessions Presented by the TMS Aluminum Committee at the 135th TMS Annual Meeting, San Antonio, TX, USA, 12–16 March 2006*; TMS: San Antonio, TX, USA, 2006; pp. 463–466.
33. Einarsrud, K.E. A Treatise on Interpolar Transport Phenomena. Ph.D. Thesis, Norwegian University of Science and Technology NTNU, Trondheim, Norway, May 2012.
34. Wang, X.; Tabereaux, A.T. Anodic Phenomena—Observations of Anode Overvoltage and Gas Bubbling During Aluminium Electrolysis. In *Light Metals 2000*; TMS: Nashville, TN, USA, 2000; pp. 239–248.